Enhanced Mechanical Properties of Uniaxially Stretched Polylactide/Poly(ethylene oxide)-*b*-poly(butylene oxide) Blend Films

Boran Zhao, Charles J. McCutcheon, Kailong Jin, Illya Lyadov, Aristotle J. Zervoudakis, Frank S. Bates, and Christopher J. Ellison**

Department of Chemical Engineering and Materials Science, University of Minnesota, Minneapolis, MN 55455, United States

*To whom correspondence should be addressed: (F.S.B.) *bates001@umn.edu*, (C.J.E.) *cellison@umn.edu*

KEYWORDS: sustainable plastics, polylactide, block copolymers, polymer blends, chain orientation, deformation mechanism, physical aging

ABSTRACT

Chain orientation, a natural consequence of polymer film processing, often leads to enhanced mechanical properties parallel to the machine extrusion direction (MD), while leaving the properties in the transverse direction (TD) unaffected or diminished, as compared to the unoriented material. Here, we report that mixing poly(ethylene oxide)-*block*-poly(butylene oxide) (PEO-PBO) diblock copolymer that forms dispersed particles in an amorphous polylactide (PLA) matrix produces uniaxially stretched blend films with enhanced toughness in both the MD and TD. Small-angle X-ray scattering experiments and visual observations revealed that the dominant deformation mechanism for blend films transitions from crazing to shear yielding in the MD as the stretching ratio increases, while crazing is the primary deformation mechanism in the TD at all stretching ratios investigated. As the films age at room temperature, crazing becomes more prevalent in the MD without compromising the improved toughness. The stretched blend films were susceptible to some degree of mechanical aging in the TD but remained 5-fold tougher than stretched neat PLA films for up to 150 days. This work presents a feasible route to produce uniaxially stretched PEO-PBO/PLA films that are mechanically tough which provides a more sustainable plastic alternative.

INTRODUCTION

The US plastic packaging industry, ~$40 billion in 2020[1], is dominated by petroleum-based polymers that are not easily degraded or recycled. This problem is exacerbated by a preponderance of single-use applications leading to an accelerating buildup in landfills, ~10 million US tons in 2018.[2] Thus, sustainable plastics that can be composted or recycled without compromising performance are highly attractive.[3-5] Polylactide (PLA) is one alternative of interest as it is sustainable, bio-sourced, industrially compostable and commercially produced with an annual

global production of 190,000 tons in 2019.[6] However, applications of PLA are greatly limited by fast physical aging (within hours of melt processing), which results in embrittlement.[7-11]

One strategy to toughen PLA is by chain orientation, which is commonly achieved through film stretching processes, such as in blown or cast film extrusion.[12] For most processes, chain orientation occurs predominately in the direction of extrusion, referred to as the machine direction (MD), in order to maximize the throughput and/or downgauge sheet/film thickness. Previous studies[13-16] have shown that uniaxial stretching reduces the activation energy for plastic flow (shear yielding), leading to ductile deformation when mechanically tested parallel to the chain orientation direction. In contrast, mechanical properties in the perpendicular or transverse direction (TD) typically remain the same or diminish compared to the unoriented material.[14, 17] Biaxial orientation/stretching can be employed to balance the properties in the MD and TD,[18] however such processing requires sophisticated equipment and a meticulous stretching procedure, increasing the cost of biaxially oriented films compared to uniaxial analogs.[19, 20] Therefore, methods to produce uniaxially stretched tough films that have balanced properties in both the MD and TD are highly desirable.

Another effective method to toughen PLA is to blend it with certain diblock copolymers. In previous studies on molded bulk systems, poly(ethylene oxide)-*block*-poly(butylene oxide) (PEO-PBO)[21-23] was used as an effective additive to toughen PLA. The PBO block drives phase separation due to its incompatibility with PLA while the presence of the PEO block promotes interfacial activity, leading to uniformly dispersed, sub-micron size, rubbery particles that are stable to static thermal anenaling.[21] Several advantages of the PEO-PBO additive for PLA have been demonstrated including maintaining optical transparency due to refractive index matching and low mass loading requirement (less than 5 wt %) for significant mechanical property

improvements over neat PLA accompanied by minimal decrease in the Young's modulus (less than 10%). While some research has investigated stretching of films containing rubbery particles, most studies have focused on the impact of chain orientation on toughening in the MD;[24-29] only a few studies have investigated the influence of chain orientation on the mechanical properties and deformation mechanism in the TD.[30] Similar to neat oriented polymers, stretched films blended with rubbery particles often exhibit improved toughness only in the MD.

Driven by the need to produce sustainable PLA films that are tough in both the MD and TD, we investigated uniaxially stretched PEO-PBO/PLA blend films. First, we chose the amorphous instead of semi-crystalline grade of PLA in this study to focus on the effect of chain orientation (in the absence of crystalline domains) on the mechanical performance and deformation mechanism of the PEO-PBO/PLA blends; although the semi-crystalline grade PLA generally yields better gas barrier properties, amorphous PLA is more degradable and useful in applications requiring transparency. Second, both neat and blend films were stretched to a series of stretching ratios (up to 800% of the original length) to cover a full spectrum of chain orientation possibilities. Lastly, films were stretched at slightly elevated temperatures (i.e., ~10 °C above the glass transition temperature, T_g) followed by fast quenching to room temperature (RT) to ensure affine chain deformation. The mechanical performance of the stretched films was characterized by conducting room temperature tensile testing in both the MD and TD. Visual inspection and small angle X-ray scattering were carried out during tensile testing to investigate the deformation processes and understand the deformation mechanism. Moreover, the effect of aging on the mechanical performance of the stretched films was closely monitored as a function of time up to ~150 days in both MD and TD to better understand longer term performance.

EXPERIMENTAL SECTION

Materials. Amorphous-grade PLA (Ingeo™ 4060D; absolute number average molar mass, M_n = 83 kg/mol with a dispersity, $Đ$ = 1.53) and diblock copolymer (PEO-PBO; PEO volume fraction = 0.35, M_n = 7.4 kg/mol and $Đ$ = 1.05) with trade name Fortegra™ 100 were purchased from NatureWorks and Olin Corporation, respectively. All chemicals were used as received. The molecular characteristics of PLA and PEO-PBO are summarized in **Table S1**.

Blend preparation and thermal properties. A PEO-PBO/PLA blend containing 3 wt % PEO-PBO was prepared using a masterbatch-dilution method.[21] Neat PLA was first melt blended with PEO-PBO in a twin screw extruder (PRISM, 16 mm screw diameter with L:D = 24:1) yielding a 10 wt % concentrated masterbatch. The twin screw extruder was operated at 60 rpm and the operating temperatures (from hopper to die) were set to 90 °C, 120 °C, 160 °C and 180 °C. The extrudate was cooled with a room temperature water bath, pelletized, and dried in a vacuum oven at 40 °C for 48 hr. Then the PEO-PBO/PLA masterbatch was dry mixed with a pre-determined amount of neat PLA pellets and processed following the same extrusion parameters as the masterbatch resulting in a 3 wt % PEO-PBO/PLA blend. The T_g for all materials were obtained by differential scanning calorimetry (DSC). See **Supporting Information** for detailed procedures.

Compression molding. To prepare isotropic samples for stretching experiments, 500-µm-thick neat PLA and PEO-PBO/PLA blend sheets were prepared by compression molding. Polymer pellets were sandwiched between two Teflon films (American Durafilm) with 500-µm-thick steel spacers in between, molded in a Carver hydraulics press at 150 °C for 5 min and quenched (in a hydraulic press with water cooling) to room temperature (RT) within 30 sec. The sheets were cut into 90 mm × 90 mm squares with 10 mm grids drawn using a Sharpie pen. The grids provided a visual guide to assess the stretching uniformity.

Film stretching. Stretching of the isotropic PLA and PEO-PBO/PLA sheets was carried out with a laboratory stretching machine (KARO IV) at 70 °C at the University of Akron. The square sheets were clamped on all sides (5 clamps on each side), heated to 70 °C in 120 s, and stretched at 0.05 s^{-1} to the target stretching ratio (λ) defined by:

$$\lambda = \frac{L}{L_0} \tag{1}$$

where L is the length of the stretched film and L_o is the initial length of the isotropic sheet prior to stretching. The width of the films was held constant during stretching while the thickness was allowed to freely decrease. The force and stretching ratio were simultaneously recorded. After stretching, the film was cooled to RT with air within 1 min. The stretched films are labeled as (N/B)Uλ(M/T) where N/B stands for either neat PLA (N) or 3 wt % PEO-PBO/PLA blend (B) films, U stands for uniaxial stretching, λ represents the stretching ratio and M/T indicates the testing direction in either MD (M) or TD (T). For example, NU1T stands for a neat unoriented PLA film tested in the TD. BU4M represents a 3 wt % PEO-PBO/PLA blend film uniaxially stretched to λ = 4 and tested along the MD. In some cases, "λ" appears in the label, which refers to all specimens tested in a certain direction. For example, NUλM represents all neat PLA films tested in the MD. In addition, NU1M/T and BU1M/T stand for unstretched/isotropic neat and blend films.

Film shrinkage ratio measurement. To characterize the degree of orientation, the stretched films were immersed in a silicone oil bath at 70 °C for 1 hr and allowed to shrink freely. The dimensions in the stretching direction before and after shrinkage were measured and reported as the shrinkage ratio,

$$\lambda_k = \frac{L}{L_k} \tag{2}$$

where L and L_k represent the film length before and after shrinking.

Film morphology characterization. The morphology of PEO-PBO particles in isotropic and stretched films was assessed using a Hitachi S-4700 scanning electron microscopy (SEM). The isotropic samples were cryo-fractured in liquid nitrogen (LN_2) then rinsed with methanol to remove PEO-PBO, dried in vacuum oven at room temperature, and finally sputter coated with 5 nm of iridium before SEM characterization. Due to the small thickness, we focused on the surface instead of the cross-sectional area of the stretched films. The stretched films for SEM were prepared the same way as the isotropic samples. The films were rinsed quickly with methanol and then immediately air dried to prevent any solvent induced shrinkage. The aspect ratios of the PEO-PBO particles were analyzed using ImageJ from at least 20 particles.

Tensile testing. Room temperature tensile tests were performed on an Instron 5966 universal tester at 1 mm/min according to ASTM D1708. Tensile specimens were prepared using a dumbbell cutter (Dumbbell Co., Ltd. SDL200, equipped with an SDMK-1000 dumbbell cutter). All mechanical properties were averaged over at least 4 specimens for films aged $\leq$ 4 days; it is noteworthy that mechanical properties were not significantly different between 2 and 4 days of aging. Due to the limited availability of films, less than 3 specimens were averaged at certain aging times.

Small angle x-ray scattering (SAXS). 2-dimensional SAXS patterns were obtained from a Ganesha 300 XL SAXS system (SAXSLAB) with an X-ray wavelength λ = 1.54 Å. Tensile tests were performed in-situ using a Linkam tensile stage fitted with a 200 N load cell. The experiments were performed on standard dog bone shaped specimens and the experimental setup is shown in **Figure S1**. The samples were stretched at 1 mm/min to a specified strain (either 10 % or 40 % strain), then the samples were held at constant strain and exposed to X-rays for 5 min. An example of the resulting stress-strain and stress-time data is displayed in **Figure S2**. 2D SAXS patterns

were integrated over azimuthal angles from 15° to -15° (perpendicular to the strain direction of 90°) producing a 1D plot of intensity vs scattering wave vector, $q = 4\pi\lambda^{-1}\sin(\theta/2)$. The intensity was normalized by sample thickness to make relative comparisons between samples.

RESULTS AND DISCUSSION

Film stretching and morphology of stretched films.

Figure 1 shows a schematic of the preparation of uniaxially stretched films in this study; this process simulates common film producing practices, e.g., via blown- and cast-film extrusion.[19] Briefly, 3 wt % PEO-PBO was melt blended with amorphous PLA and the resulting blends were compression molded into 500 μm thick isotropic sheets as shown in **Figure 1a** and **1b**. Then the sheets were stretched uniaxially to a series of λ at 70 °C, one example is shown in **Figure 1c** using the stretching setup shown in **Figure 1d**. The thermal properties of the materials before stretching are summarized in **Table S2** and **Figure S3**. Although the PEO-PBO additive is phase-separated from the PLA matrix primarily forming dispersed droplets (see later in this section), the T_g decreased from 56 °C for neat PLA to 53 °C for the 3 wt % PEO-PBO/PLA blend, indicating a minor plasticization effect of PEO-PBO likely due to partial miscibility of PEO-PBO with PLA. The images of the stretched neat and blend films are displayed in **Figure S4**. The measured λ values by analysis of grid line changes are in good agreement with the target values (stretching machine settings), as shown in **Figure S5**.

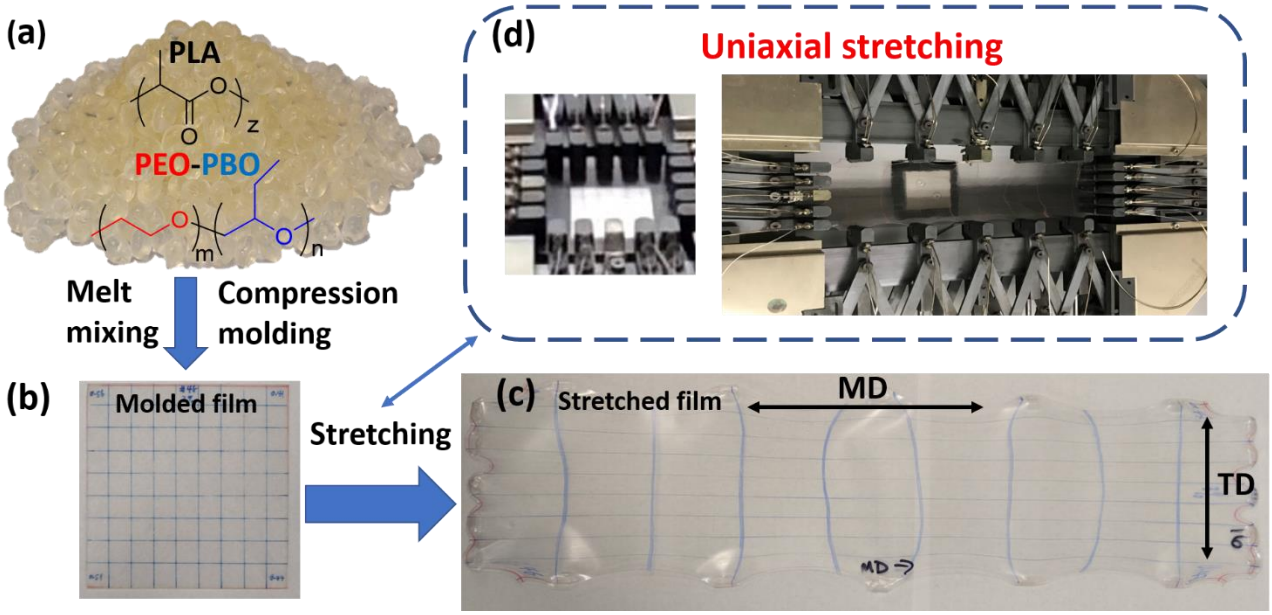

Figure 1. The processing procedure for uniaxially stretched films. (a) PLA pellets and chemical structures of PLA and PEO-PBO. (b) An isotropic sheet sample prepared by compression molding, with gridlines drawn to visually indicate the uniformity after stretching. (c) A stretched film (BU6) where MD and TD are labeled as guidelines. (d) Configurations of the stretching setup before (left) and after (right) uniaxial stretching.

Both the stretching force and λ were measured during film stretching and representative data for neat PLA and PEO-PBO/PLA blends are shown in **Figure 2a** and **2b**, respectively. These results depict an overall macroscopic material behavior during stretching. In general, the force vs λ data overlays well with increasing λ across separate samples, indicating consistent stretching results. The stretching force increases nearly linearly with λ before reaching a peak value at λ = 1.8, which signifies the onset of strain softening. At λ = 6 both the neat PLA and PEO-PBO/PLA films exhibit a strain-softening to strain-hardening transition. Microscopically, PLA chains are increasingly stretched with increasing λ, leading to chain orientation along the stretching direction.

Chain orientation was "fixed" into the samples by rapidly quenching the films to $T < T_g$ after stretching. The degree of chain orientation in amorphous polymers can be quantified by several techniques including infrared spectroscopy (IR),[31, 32] polarized optical microscopy (POM),[33, 34] and film shrinkage ratio.[35-37] Shrinkage ratio measurements were adopted in this study due to the variance in film thickness which could complicate the application of IR or POM. As shown in **Figure 2c**, λ_k corresponds closely to λ up to $\lambda = 4$, then deviates at larger λ values, which is likely a result of chain sliding and disentanglement processes at larger λ.[38, 39] This deviation is more pronounced in PEO-PBO/PLA films, which could be attributed to a plasticization effect of PEO-PBO. Greater chain mobility in these films may facilitate chain sliding and disentanglement. This is further supported by PEO-PBO/PLA films reaching $\lambda = 8$ at a lower drawing force compared to neat PLA films which ruptured at $\lambda \approx 7$.

Figure 2d reveals that PEO-PBO forms droplets which are dispersed in the PLA matrix during melt mixing (before stretching). The morphology indicates phase separation of PEO-PBO for reasons mentioned earlier and consistent with previous work.[21] **Figure 2e** displays a representative surface morphology of the stretched blend films. The full suite of SEM micrographs of the stretched blend films is shown in **Figure S6.** Significant particle deformation occurs during stretching as the initially sphere-like PEO-PBO particles are elongated along the MD. The deformation of PEO-PBO particles was quantified by their aspect ratio (long axis/short axis), which is found to scale proportionally with λ as shown in **Figure 2f**.

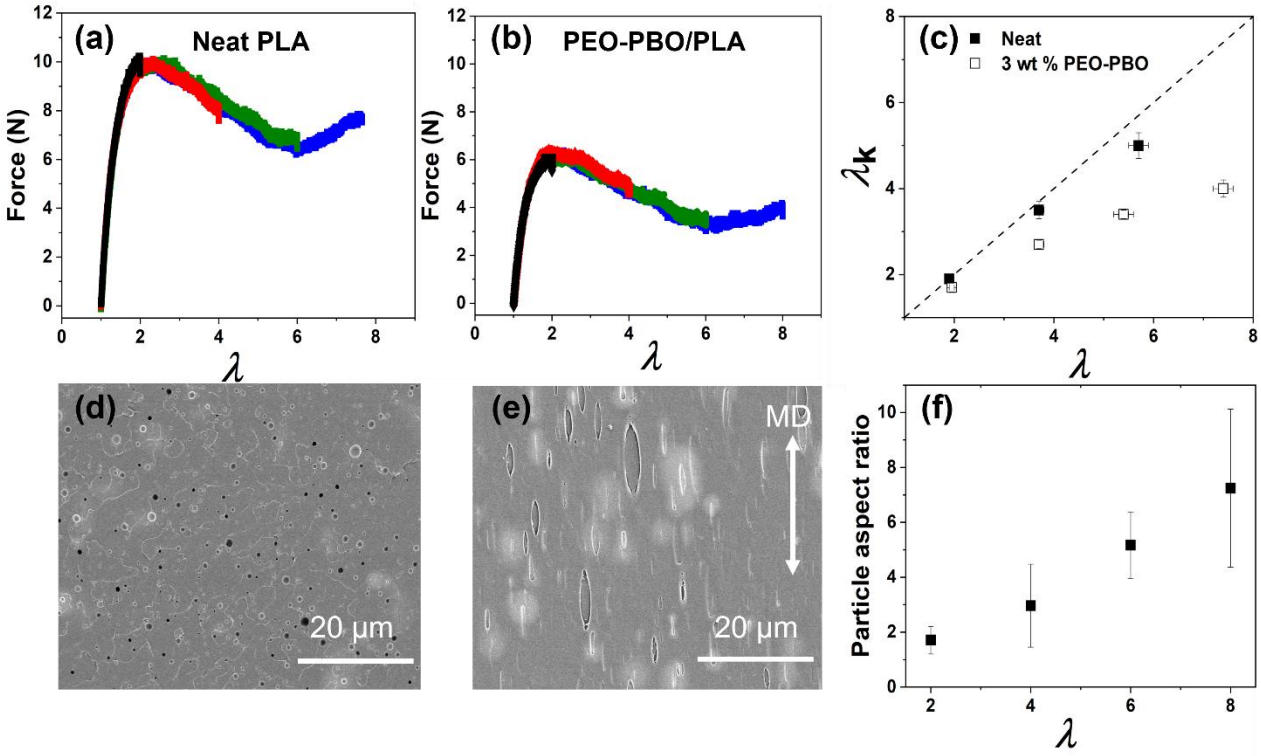

Figure 2. Stretching force values as a function of stretching ratio during film stretching at 70 °C for (a) neat PLA films and (b) PEO-PBO/PLA blend films. Different colors signify separate samples stretched to different λ values. (c) Film shrinkage ratio values for neat PLA and PEO-PBO/PLA blend films at different stretching ratios; values in the x-axis represents measured average stretching ratios. Representative SEM images of PEO-PBO particle morphologies for (d) unoriented (BU1M/T) and (e) stretched (BU6) PEO-PBO/PLA films. (f) Particle aspect ratio values for stretched PEO-PBO/PLA blend films at different target stretching ratios. The error bars in (c) and (f) represent one standard deviation about the mean from at least 3 films or 50 particles.

Mechanical properties

Room temperature tensile experiments (ASTM D1708) were performed on neat and blend films to explore the effects of chain orientation on the mechanical properties. Representative engineering stress-strain data and mechanical properties in the MD and TD are displayed through **Figure 3-5**,

respectively. The results are also summarized in **Table 1**. When examined in the MD, the Young's modulus (E) and yield stress (σ_Y) increase monotonically with λ for both neat PLA (coded as NUλM) and PEO-PBO/PLA blends (coded as BUλM) films, as shown in **Figure 4a,b**. The elongation at break (ε_B) for NUλM films (**Figure 4c**) increases significantly with increasing λ from 9 ± 4 % at λ = 1 to 128 ± 25 % at λ = 2, indicating that chain orientation transforms PLA from a brittle to a ductile plastic. However, as λ is increased further, from 2 to 6, ε_B decreases from 128 ± 25 % to 34 ± 6 %. We hypothesize that this is related to the overall chain stretching ratio (λ_e) approaching the theoretical stretching limit (λ_{max}), which is defined by,[40]

$$\lambda_e = \lambda_k(1 + \varepsilon_B) \tag{2}$$

$$\lambda_{max} = l_e/d \tag{3}$$

where l_e is the chain contour length between entanglements and d is the entanglement mesh size. For PLA, l_e = 46 nm and d = 6.9 nm (see **Supporting Information** for detailed calculations and associated assumptions).[21, 41] λ_e represents the total amount of chain extension from both film stretching and tensile testing, while λ_{max} is constrained by chain entanglements. This argument is supported by the results summarized in **Table 1**, where λ_e gradually increases with λ and approaches $\lambda_{max} \approx 7$.

Turning to the blend films, BU1M/T is significantly tougher than NU1M/T, which is consistent with our previous work.[21, 22] As λ increases from 1 to 8, ε_B decreases monotonically from ~ 200% to ~ 35%, which is attributed to λ_e being limited by λ_{max}, similar to the NUλM films. It is worth noting that at the same λ, ε_B and the overall tensile toughness of the BUλM films are always larger than those of the NUλM films, as shown in **Figure 4c**,**d**. This is likely a result of less chain orientation characterized by a lower λ_k for BUλM films compared to NUλM films, allowing the tensile specimens to elongate to larger strains. Another potential reason is the partial miscibility of

PEO-PBO in PLA,[21] allowing the specimens to plastically deform and elongate to larger strains. Moreover, phase separated PEO-PBO particles act as stress concentrators which also promotes localized plastic deformation.[42]

In contrast to the greatly improved ductility of the NUλM films, neat PLA films tested in the TD (NUλT films) remain brittle, failing at $\varepsilon_B < 10\%$ regardless of λ (**Figure 3c**). Also, there is a continuous decrease in E and σ_Y with increasing λ (**Figure 5a,b**), indicating the integrity of the PLA chain entanglement network gradually diminishes with stretching.[17] However, stretched PEO-PBO/PLA films tested in the TD (BUλT films) exhibit remarkable ductility (**Figure 3d**), displaying at least 10-fold greater toughness than the corresponding NUλT films (**Figure 5c,d**). Therefore, uniaxially stretched PEO-PBO/PLA films exhibit comparable toughness in both the MD and TD, which is a highly desirable feature for film packaging and other applications.

Table 1. Summary of mechanical properties of neat PLA and PEO-PBO/PLA films.[a]

Samples	Testing direction	λ	E (GPa)	σ_Y (MPa)	ε_B (%)	Toughness (MJ/m^3)	λ_e
NU1M/T	-	1	3.0 ± 0.1	51 ± 2	9 ± 4	3.0 ± 2.0	1
NU2M	MD	2	3.1 ± 0.1	66 ± 2	130 ± 25	59 ±13	4.3
NU4M	MD	4	3.4 ± 0.2	65 ± 5	70 ± 14	39 ± 14	6.0
NU6M	MD	6	3.9 ± 0.2	78 ± 6	34 ± 6	25 ± 3	6.7
NU2T	TD	2	3.0 ± 0.1	55 ± 1	6 ± 4	2.4 ± 1.5	1
NU4T	TD	4	2.8 ± 0.1	46 ± 1	6 ± 3	2.0 ± 1.5	1
NU6T	TD	6	2.7 ± 0.1	41 ± 2	5 ± 1	1.7 ± 0.5	1
BU1M/T	-	1	2.8 ± 0.1	35 ± 4	200 ± 46	45 ± 12	3.0
BU2M	MD	2	3.1 ± 0.1	60 ± 3	160 ± 2	69 ± 1	4.4
BU4M	MD	4	3.1 ± 0.1	66 ± 1	100 ± 19	58 ± 11	5.5
BU6M	MD	6	3.3 ± 0.2	63 ± 2	78 ± 18	44 ± 10	6.1
BU8M	MD	8	3.4 ± 0.2	84 ± 1	35 ± 1	25 ± 4	5.4
BU2T	TD	2	2.8 ± 0.1	38 ± 2	280 ± 20	86 ± 6	3.8
BU4T	TD	4	2.6 ± 0.4	31 ± 1	250 ± 14	67 ± 6	3.5
BU6T	TD	6	2.7 ± 0.1	26 ± 1	150 ± 49	34 ± 10	2.5
BU8T	TD	8	2.5 ± 0.1	27 ± 1	150 ± 36	36 ± 9	2.5

[a] ± represents one standard deviation about the mean, based on at least 4 replicates for each sample.

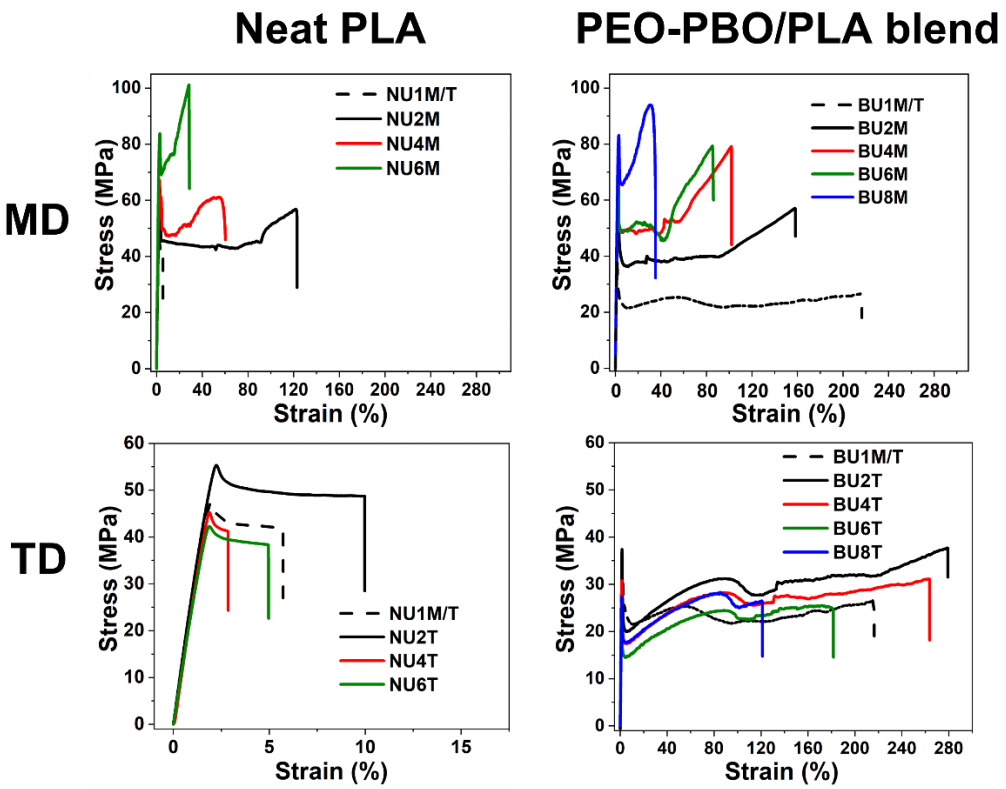

Figure 3. Representative engineering room temperature stress-strain data from neat PLA and PEO-PBO/PLA blend films tested in the MD and TD, respectively.

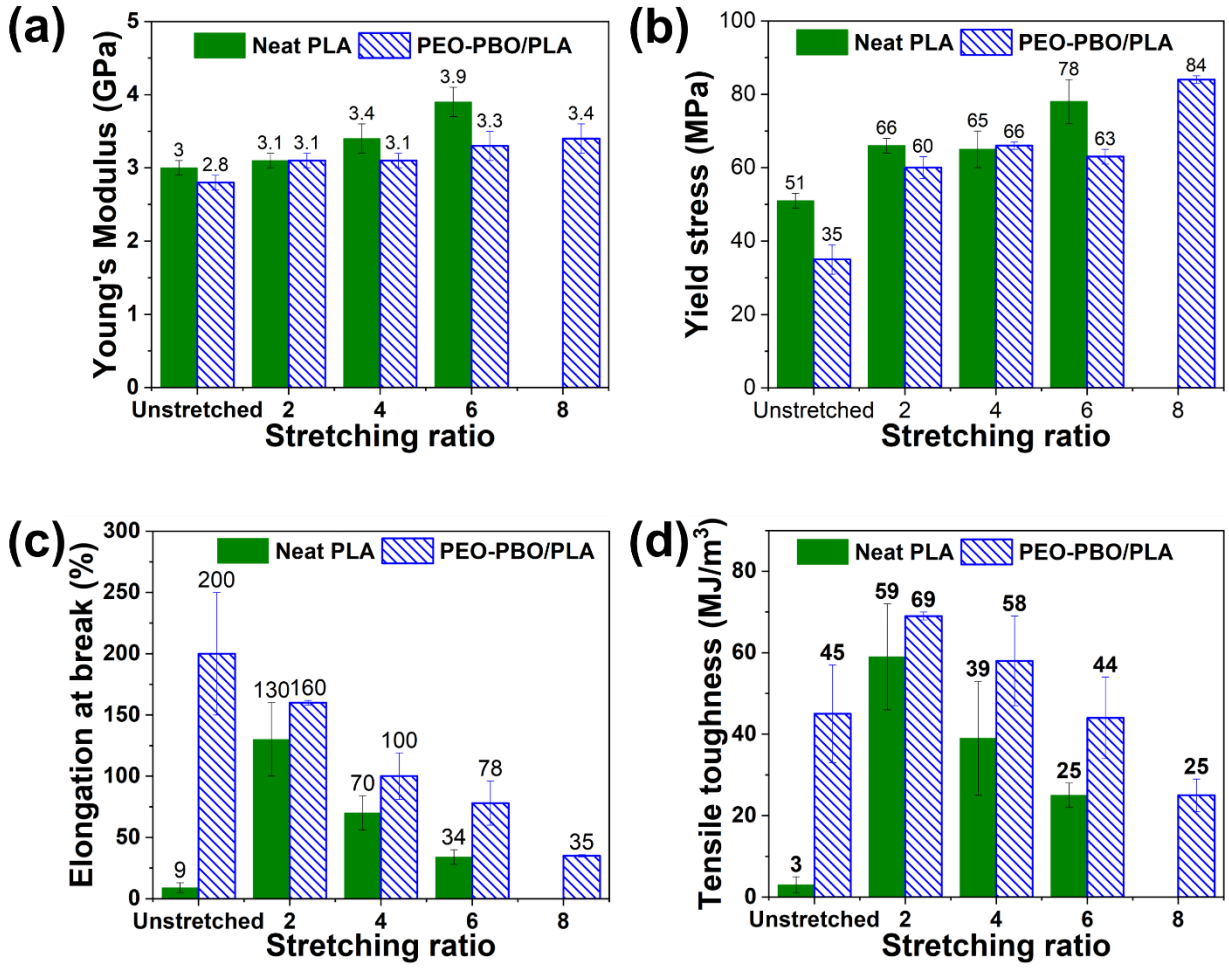

Figure 4. Summary of (a) Young's modulus, (b) yield stress, (c) elongation at break and (d) tensile toughness data examined in the MD. Due to time constraints, tensile tests were conducted on PLA and PEO-PBO/PLA after 2 and 4 days of aging, respectively. The mechanical properties of neat PLA and PEO-PBO/PLA blend films can be compared despite this difference in aging time due to a negligible variation in the mechanical properties of the blended specimens during the first week of aging.

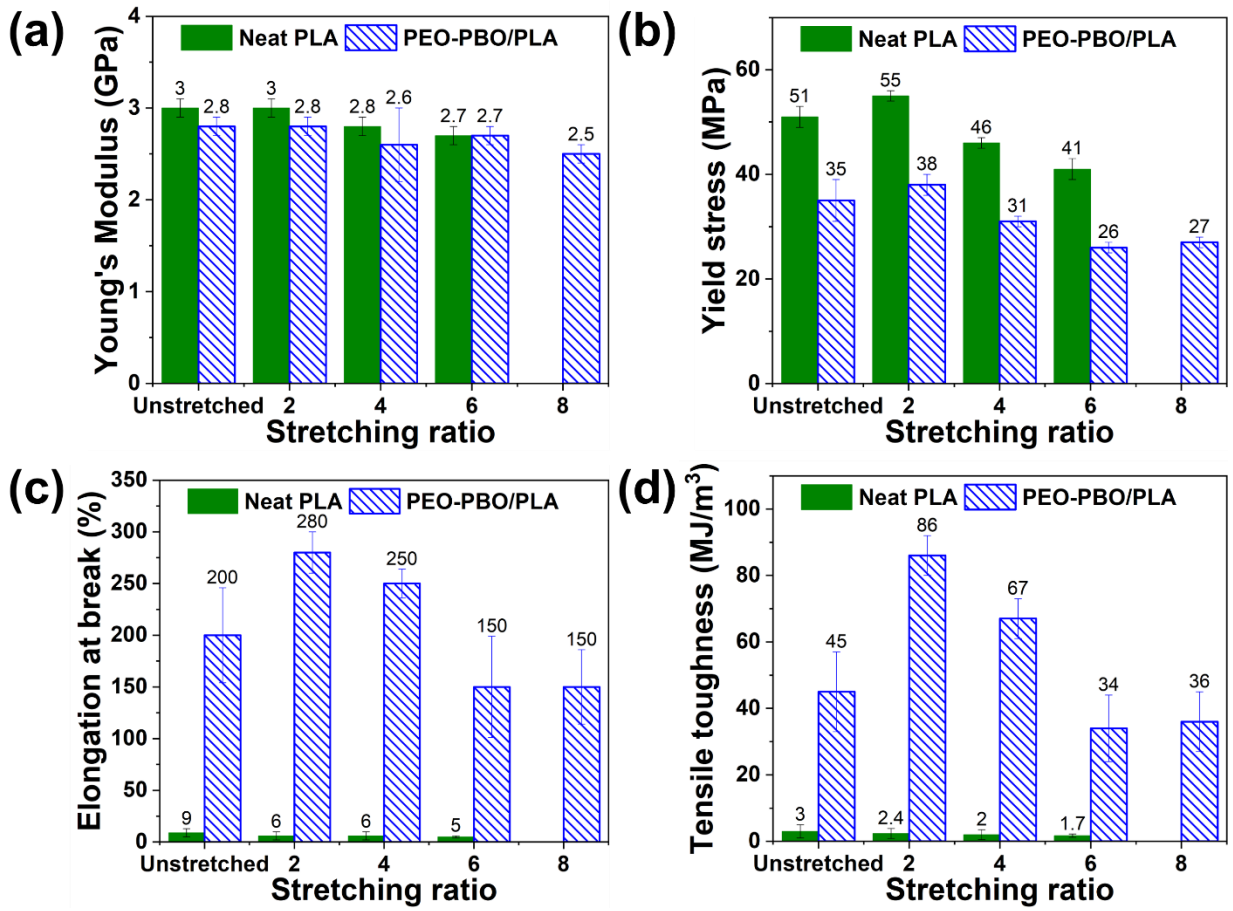

Figure 5. Summary of (a) Young's modulus, (b) yield stress, (c) elongation at break and (d) tensile toughness data examined in the TD. Due to time constraints, tensile tests were conducted on PLA and PEO-PBO/PLA after 2 and 4 days of aging, respectively. The mechanical properties of neat PLA and PEO-PBO/PLA blend films can be compared despite this difference in aging time due to a negligible variation in the mechanical properties of the blended specimens during the first week of aging.

Toughening mechanism

Macroscopic deformation. Neat and blend film tensile specimens were photographed at various stages of deformation. Brittle NU1M/T and NUλT films display a few localized white streaks

perpendicular to the tensile direction before failing (**Figure S7**), which we attribute to light scattering from craze voids. In contrast, **Figures S8-S10** display the deformation processes of NU2M, NU4M, and NU6M, which undergo necking with limited whitening in the gauge area. We note that necking propagates through the gauge area more readily with increasing λ as highlighted in **Figure 6a**. By 40% tensile strain, necking had propagated through the entire gauge area for NU6M, while at the same strain necking was still developing in the NU2M and NU4M films. These observations suggest that orientation allows chains to slide by one another more easily, leading to ductile deformation by shear yielding with increasing λ.

While all NUM films deform by shear yielding, the deformation mechanism of BUM films is strongly dependent on λ. **Figure S11** displays photographs of the gauge section of BU2M films at various strains. Uniform whitening of the gauge area occurs at the yield point and elongation proceeds by volume expansion prior to necking, evidenced by the relatively constant width and thickness (estimated visually). Similar behavior characterizes BU1M/T films. This is attributed to cavitation of the PEO-PBO particles, which facilitates uniform crazing.[21] After necking (or uniform plastic deformation) the films deform by shear yielding until failure. However, at $\lambda \geq 4$ there is a distinct change in the deformation mechanism as shown in **Figure 6b**. The most striking difference for films with larger λ values (BU4M through BU8M, **Figure S12-S14**) compared to films with $\lambda \leq 2$ (BU1M/T and BU2M) is thinning of the gauge area and sample transparency, indicating the samples are not forming voids or crazes, rather they are deforming by shear yielding.

In contrast to the BUλM films, the deformation process for BUλT films does not change with λ (**Figures S15**) and crazing is the dominant deformation mechanism. We observed that BUλT films display delayed necking compared to BU1M/T and BU2M films, in other words, a prolonged crazing process, as illustrated in **Figure 7**. It is worth reiterating that unstretched BU1M/T, BUλT

and BU2M films all undergo uniform crazing before necking. This observation complements the findings in **Figure 6** where crazing is suppressed when the initial chain orientation is parallel to the tensile strain direction and suggests that crazing is promoted when the initial chain orientation is perpendicular to the tensile strain direction.

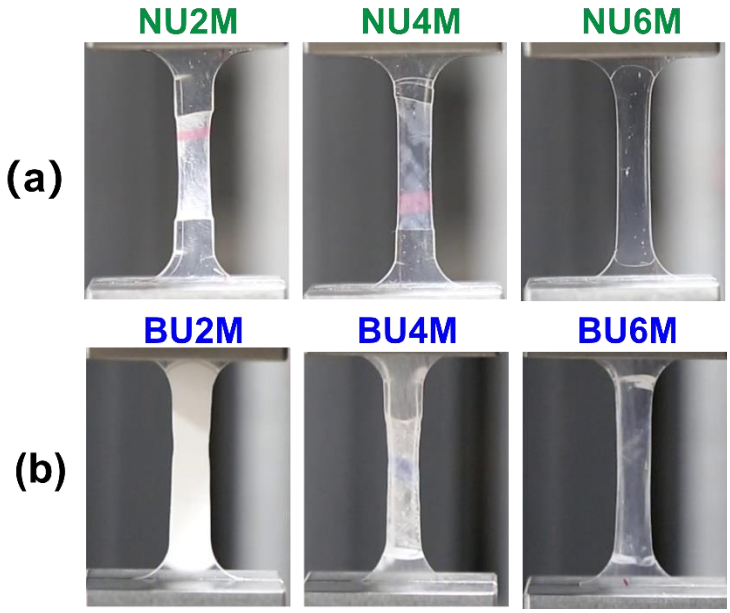

Figure 6. Representative gauge area images of (a) NUλM and (b) BUλM films elongated to 40 % tensile strain during tensile tests, highlighting the macroscopic deformation process.

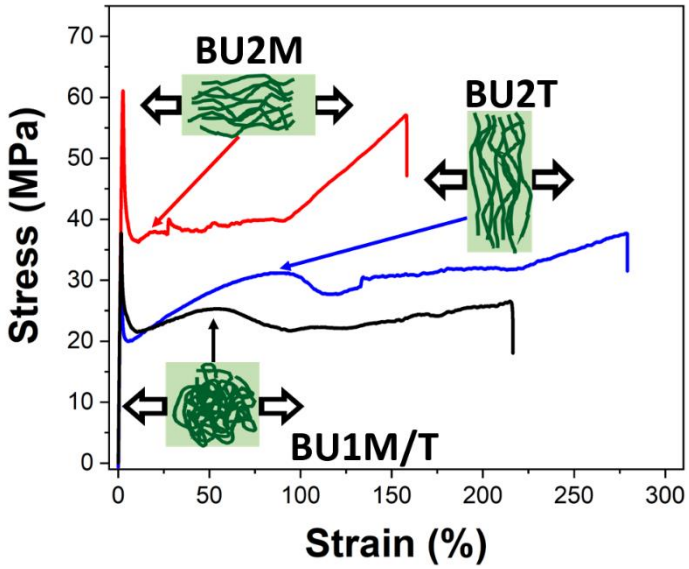

Figure 7. Representative engineering stress-strain data for BU1M/T, BU2M, and BU2T films, indicating a shift of necking caused by chain orientation. The necking transition is identified by the color-coded arrows. The chain orientation relative to the tensile strain direction (horizontal black arrows) are provided as inserts.

Microscopic deformation (SAXS). Deformation mechanisms were further evaluated by small-angle X-ray scattering (SAXS) experiments. 2D SAXS patterns for NUλM and BUλM films elongated to 40 % strain are displayed in **Figure S16a,b**; information about the in-situ tensile apparatus is provided in **Figure S1** and **S2**. Among the NUλM films, only NU2M displays a weak equatorial scattering pattern, which is attributed to crazing induced by local variance in chain density or intrinsic impurities. NU4M and NU6M display almost no scattering, consistent with deformation dominated by shear yielding. For BUλM films, there is a dramatic change in the 2-D SAXS patterns with λ, which is consistent with the photographs of the gauge areas (**Figures S11-S14**). BU2M films display a typical craze scattering pattern with scattering intensity in the meridional (90°, parallel to the strain direction) and equatorial (0°, perpendicular to the strain direction) axes. We associate the intense meridional scattering with cavitated PEO-PBO particles

and voids from crazing, while the equatorial scattering is attributed to the formation of craze fibrils parallel to the strain direction. At larger values of λ there is almost no scattering intensity, indicative of deformation by shear yielding as opposed to crazing. These differences were further quantified by calculating the scattering invariant, Q_0, along the equatorial axis (across the azimuthal angles -15° to 15°) (see **Supporting Information**). The magnitude of Q_0 is proportional to the craze volume (V) as described elsewhere.[21, 22] As shown in **Figure 8a**, only BU2M exhibits a large Q_0, which increases with strain, while the other stretched films (both neat and blend films) generated limited scattering intensity. Note: despite the weak equatorial pattern found in NU2M, NUλM films display similar Q_0 values due to normalization of the scattering intensity by specimen thickness. Q_0 was also determined for BUλT films (**Figure 8b)** and found to be relatively constant at all λ values, indicating that crazing is the dominant deformation mechanism. These observations in the MD can be attributed to an increase in the craze stress (σ_{cz}) with increasing λ. σ_{cz} of a stretched film is defined by[22]

$$\sigma_{\mathrm{cz}} = \sigma_{cz}^{iso} + \frac{\sigma_{conf}}{\beta} \tag{4}$$

where σ_{cz}^{iso} is the craze stress for isotropic films, σ_{conf} is the conformational stress associated with the fixed stress after film stretching then quenching, and β is a geometric constant smaller than 1.[35, 41] The parameter σ_{conf} is proportional to λ_{k},[35, 43]

$$\sigma_{conf} = G_e(\lambda_k^2 - \frac{1}{\lambda_k}) \tag{5}$$

where G_{e} represents the elastic modulus associated with entanglements. (See **Table S3** and **Supporting Information** regarding the detailed calculations and assumptions). A comparison between σ_{cz} and σ_{Y} for BUλM films is provided in **Figure S17**. Whether plastic deforms by shear yielding or crazing is believed to depend on which stress condition is reached first.[44] Increasing λ causes σ_{cz} to exceed the shear yielding stress (taken as the macroscopic engineering yield stress

σ_Y) and as a consequence the films deform by shear yielding when $\lambda \geq 4$. An alternative view describes chain orientation as increasing the propensity of a material to deform by shear yielding.[14]

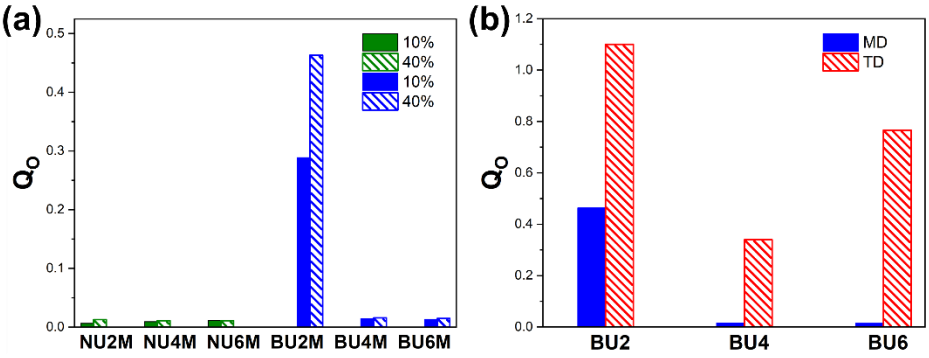

Figure 8. (a) Q_o at 10% and 40% tensile strains for NUλM and BUλM films. (b) Comparison of Q_o at 40% tensile strain for BUλM and BUλT films. Data were collected within 4 days of aging for all samples.

Mechanical properties and toughening mechanism as a function of time

Neat PLA is well known to undergo physical aging, resulting in mechanical embrittlement at room temperature after about one day following cooling from an elevated temperature. Remarkably, both NUλM and BUλM films are tough independent of aging time (i.e., elongation at break and toughness values of about 35% and 25 MJ/m^3, or greater) as shown in **Figure S18**. While NUλM films continue to deform by shear yielding with time (**Figure S19**), the deformation mechanism for BUλM films is dependent on aging. **Figure 9** displays tensile bar images of BU4M at 30% strain obtained between 4 and 96 days of aging. As the film ages, it increasingly whitens at 30% strain, and at 96 days exhibits a distinct SAXS pattern consistent with crazing, evidencing a transition from shear yielding to crazing with aging time. Similar transitions with time were also confirmed in BU6M and BU8M films as shown in **Figure S20**. As the blends age, the PLA matrix densifies, making it more difficult for chains to slide past one another during tensile deformation. This results in an increase in the shear yielding stress, which eventually exceeds the craze stress

after sufficient aging. Regardless of aging, the incorporation of PEO-PBO particles promotes the ability of BUλM films to craze in a manner that acts as a "safety net" for maintaining toughness with aging time.

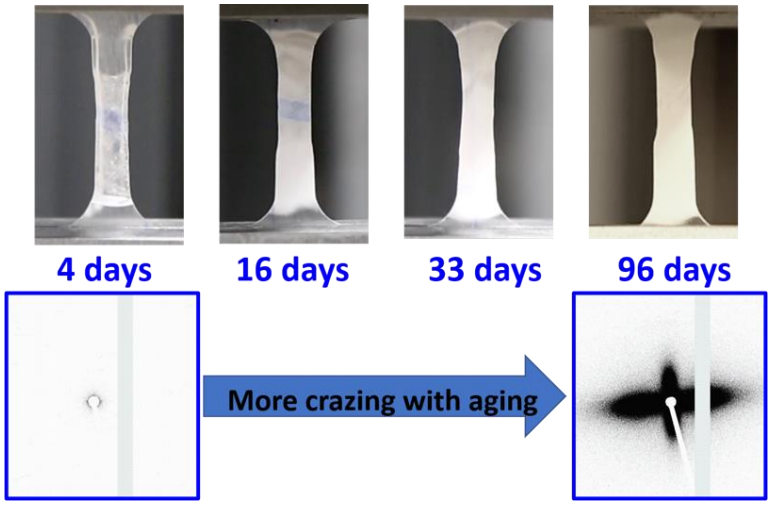

Figure 9. A series of gauge area images at 30% strain at varying aging times for BU4M films and 2D SAXS images, indicating crazing increases with time for BUλM films.

Aging also influences the BUλT films, leading to a reduction in ductility with time (**Figure 10a**). This is a surprising result because the primary deformation mechanism in the TD is crazing, which is generally accepted to be unaffected by aging[21, 45-47] and there are no apparent differences in the total volume of craze development as quantified by Q_0 (**Figure S21**). In isotropic PLA, craze fibrils form by chain disentanglement and chain scission. As crazes develop with strain, new surrounding undeformed PLA must be drawn into the craze to allow the sample to elongate. For films to craze in the TD, fibrils need to form perpendicular to the aligned chains (**Figure 10b**), this will require a complete reorientation of the chains which is facilitated by chain mobility.[35, 41] We hypothesize that this additional requirement of chain mobility for chain reorientation in the TD is heavily impacted by aging (chain densification) which causes the decrease in elongation at break and

toughness with aging time for BUλT films. There is an opportunity for future research to better understand the details of this hypothesized mechanism. Nevertheless, despite the decrease in ductility with aging time, BUλT films are at least 5-fold tougher than NUλT samples at 150 days of aging.

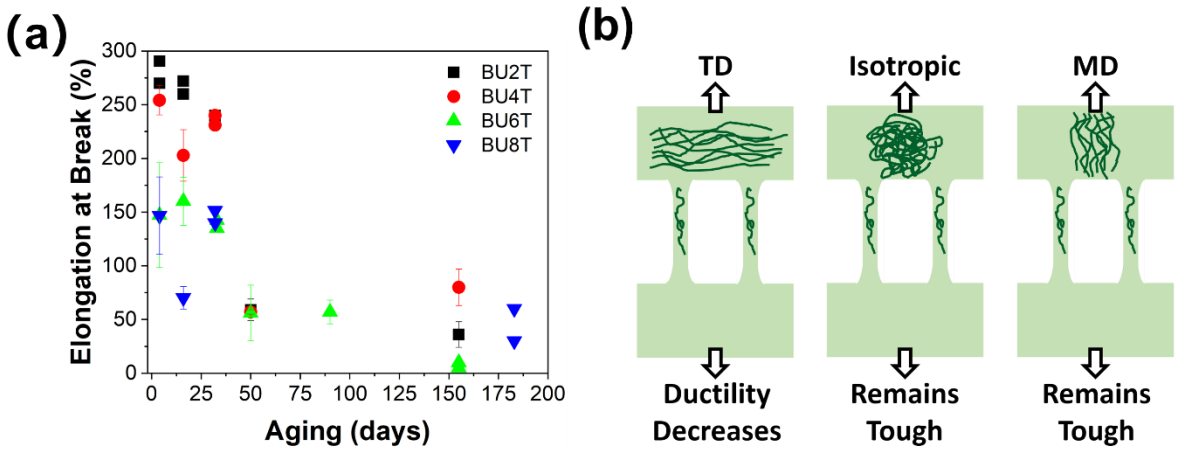

Figure 10. (a) Elongation at break for BUλT samples monitored as a function of time at room temperature. (b) A sketch of craze fibril formation relative to chain orientation. Black arrows indicates the tensile strain direction. The error bars represent one standard deviation about the mean based on at least 3 replicates for each sample. Due to limited specimen volume, certain aging time measurements were based on two replicates which are both shown without error bars to display the range of the data.

CONCLUSION

In conclusion, uniaxial stretching of both neat PLA and blend PEO-PBO/PLA films leads to tough plastics. At low aging times, NUλM films deform by shear yielding while the deformation mechanism of BUλM films depends on λ, i.e., increasing λ leads to a transition from crazing to shear yielding. However, only the blend films are tough when examined in the TD and deform by crazing. At long aging times, both

NUλM and BUλM are tough where NUλM continually deforms by shear yielding while the deformation mechanism of BUλM films transitions from shear yielding to crazing due to chain densification. The toughness of BUλT films decreases with aging time due to the increased difficulty to form craze fibrils perpendicular to the initial chain orientation direction but remains at least 5-fold tougher than NUλT films. This toughening method, a combination of melt mixing and uniaxial film stretching, can be directly integrated into common PLA film processing procedures, promoting the future applications of PLA as a sustainable material.

ASSOCIATED CONTENT

Supporting Information

Material details; blend preparation and film stretching procedure; shrinkage and tensile testing method; thermal properties; gauge area images of deformed tensile bars of neat PLA and blend stretched films in both MD and TD; morphology characterization; assumptions and calculation of λ_{max} and σ_{cz}; mechanical properties of NUλM at long aging time; and SAXS experimental setup.

AUTHOR INFORMATION

Corresponding Authors

Frank S. Bates − Department of Chemical Engineering and Materials Science, University of Minnesota, Minneapolis, MN 55455, United States; orcid.org/0000-0003-3977-1278

Email: bates001@umn.edu

Christopher J. Ellison − Department of Chemical Engineering and Materials Science, University of Minnesota, Minneapolis, MN 55455, United States; orcid.org/0000-0002-0393-2941

Email: cellison@umn.edu

Authors

Boran Zhao − Department of Chemical Engineering and Materials Science, University of Minnesota, Minneapolis, MN 55455, United States; orcid.org/0000-0002-4508-8451

Charles J. McCutcheon − Department of Chemical Engineering and Materials Science, University of Minnesota, Minneapolis, MN 55455, United States; orcid.org/0000-0002-2553-4012

Kailong Jin − Department of Chemical Engineering and Materials Science, University of Minnesota, Minneapolis, MN 55455, United States; orcid.org/0000-0001-5428-3227

Illya Lyadov − Department of Chemical Engineering and Materials Science, University of Minnesota, Minneapolis, MN 55455, United States; orcid.org/0000-0002-2142-5185

Aristotle J. Zervoudakis − Department of Chemical Engineering and Materials Science, University of Minnesota, Minneapolis, MN 55455, United States; orcid.org/0000-0002-4758-1784

Author Contributions

BZ and CJM are co-first authors. The manuscript was written through contributions of all authors. All authors have given approval to the final version of the manuscript.

Notes

The authors declare no competing financial interest.

ACKNOWLEDGMENTS

This work was supported primarily by the farm families of Minnesota and their corn check-off investment, and in part by the National Science Foundation Center for Sustainable Polymers at the University of Minnesota, a Center for Chemical Innovation (CHE-1901635). Parts of this work were carried out in the Characterization Facility at the University of Minnesota, which receives

partial support from the NSF through the MRSEC program (DMR-2011401). The film stretching experiments were conducted by Todd Lewis in the National Polymer Innovation Center (NPIC) at the University of Akron.

References

1. Kennedy, K. *Plastic Film, Sheet & Bag Manufacturing in the US*; 32611; IBISWorld, December, 2020; https://www.ibisworld.com/ (accessed 02/01/2021).

2. Containers and Packaging: Product-Specific Data. https://www.epa.gov/facts-and-figures-about-materials-waste-and-recycling/containers-and-packaging-product-specific-data (accessed 06/01/2020).

3. Miller, S. A., Sustainable Polymers: Opportunities for the Next Decade. *Acs Macro Lett* **2013,** *2* (6), 550-554. https://doi.org/10.1021/mz400207g

4. Zheng, J.; Suh, S., Strategies to reduce the global carbon footprint of plastics. *Nature Climate Change* **2019,** *9* (5), 374-378. https://doi.org/10.1038/s41558-019-0459-z

5. Millican, J. M.; Agarwal, S., Plastic Pollution: A Material Problem? *Macromolecules* **2021,** *54* (10), 4455-4469. https://doi.org/10.1021/acs.macromol.0c02814

6. Jem, K. J.; Tan, B., The development and challenges of poly (lactic acid) and poly (glycolic acid). *Advanced Industrial and Engineering Polymer Research* **2020,** *3* (2), 60-70. https://doi.org/10.1016/j.aiepr.2020.01.002

7. Haugan, I. N.; Lee, B.; Maher, M. J.; Zografos, A.; Schibur, H. J.; Jones, S. D.; Hillmyer, M. A.; Bates, F. S., Physical Aging of Polylactide-Based Graft Block Polymers. *Macromolecules* **2019,** *52* (22), 8878-8894. https://doi.org/10.1021/acs.macromol.9b01434

8. Struik, L. C. E., Physical aging in plastics and other glassy materials. *Polymer Engineering & Science* **1977,** *17* (3), 165-173. https://doi.org/10.1002/pen.760170305

9. Razavi, M.; Wang, S.-Q., Why Is Crystalline Poly(lactic acid) Brittle at Room Temperature? *Macromolecules* **2019,** *52* (14), 5429-5441. https://doi.org/10.1021/acs.macromol.9b00595

10. Cangialosi, D.; Boucher, V. M.; Alegría, A.; Colmenero, J., Physical aging in polymers and polymer nanocomposites: recent results and open questions. *Soft Matter* **2013,** *9* (36), 8619-8630. https://doi.org/10.1039/C3SM51077H

11. Pan, P.; Zhu, B.; Inoue, Y., Enthalpy Relaxation and Embrittlement of Poly(l-lactide) during Physical Aging. *Macromolecules* **2007,** *40* (26), 9664-9671. https://doi.org/10.1021/ma071737c

12. Tadmor, Z.; Gogos, C. G., *Principles of polymer processing*. John Wiley & Sons: Hoboken, New Jersey, 2013; p 705-720.

13. Guo, Y.; Peng, S.; Wang, Q.; Song, X.; Li, C.; Xia, L.; Wu, H.; Guo, S., Achieving High-Ductile Polylactide Sheets with Inherent Strength via a Compact and Uniform Stress Conduction Network. *Industrial & Engineering Chemistry Research* **2020,** *59* (26), 12096-12105. https://doi.org/10.1021/acs.iecr.0c01328

14. Razavi, M.; Cheng, S.; Huang, D.; Zhang, S.; Wang, S.-Q., Crazing and yielding in glassy polymers of high molecular weight. *Polymer* **2020,** *197*, 122445. https://doi.org/10.1016/j.polymer.2020.122445
15. Razavi, M.; Wang, S. Q., Double Yielding in Deformation of Semicrystalline Polymers. *Macromolecular Chemistry and Physics* **2020,** *221* (19), 2000151. https://doi.org/10.1002/macp.202000151
16. Gao, X.-R.; Li, Y.; Huang, H.-D.; Xu, J.-Z.; Xu, L.; Ji, X.; Zhong, G.-J.; Li, Z.-M., Extensional Stress-Induced Orientation and Crystallization can Regulate the Balance of Toughness and Stiffness of Polylactide Films: Interplay of Oriented Amorphous Chains and Crystallites. *Macromolecules* **2019,** *52* (14), 5278-5288. https://doi.org/10.1021/acs.macromol.9b00932
17. Zartman, G. D.; Cheng, S.; Li, X.; Lin, F.; Becker, M. L.; Wang, S.-Q., How Melt-Stretching Affects Mechanical Behavior of Polymer Glasses. *Macromolecules* **2012,** *45* (16), 6719-6732. https://doi.org/10.1021/ma300955h
18. DeMeuse, M. T., 5 - Other polymers used for biaxial films. In *Biaxial Stretching of Film*, DeMeuse, M. T., Ed. Woodhead Publishing: 2011; pp 47-58.
19. Baird, D. G.; Collias, D. I., *Polymer processing: principles and design*. John Wiley & Sons: Hoboken, New Jersey, 2014; p 293-297.
20. Lin, Y.; Chen, W.; Meng, L.; Wang, D.; Li, L., Recent advances in post-stretching processing of polymer films with in situ synchrotron radiation X-ray scattering. *Soft Matter* **2020,** *16* (15), 3599-3612. https://doi.org/10.1039/C9SM02554E
21. McCutcheon, C. J.; Zhao, B.; Jin, K.; Bates, F. S.; Ellison, C. J., Crazing Mechanism and Physical Aging of Poly(lactide) Toughened with Poly(ethylene oxide)-block-poly(butylene oxide) Diblock Copolymers. *Macromolecules* **2020,** *53* (22), 10163-10178. https://doi.org/10.1021/acs.macromol.0c01759
22. McCutcheon, C. J.; Zhao, B.; Ellison, C. J.; Bates, F. S., Crazing and Toughness in Diblock Copolymer-Modified Semicrystalline Poly(l-lactide). *Macromolecules* **2021,** *54* (23), 11154-11169. https://doi.org/10.1021/acs.macromol.1c01702
23. Li, T.; Zhang, J.; Schneiderman, D. K.; Francis, L. F.; Bates, F. S., Toughening Glassy Poly(lactide) with Block Copolymer Micelles. *Acs Macro Lett* **2016,** *5* (3), 359-364. https://doi.org/10.1021/acsmacrolett.6b00063
24. Liang, J. Z.; Li, R. K. Y., Rubber toughening in polypropylene: A review. *J Appl Polym Sci* **2000,** *77* (2), 409-417. https://doi.org/10.1002/(SICI)1097-4628(20000711)77:2<409::AID-APP18>3.0.CO;2-N
25. Wang, Y.; Xiao, Y.; Zhang, Q.; Gao, X.-L.; Fu, Q., The morphology and mechanical properties of dynamic packing injection molded PP/PS blends. *Polymer* **2003,** *44* (5), 1469-1480. https://doi.org/10.1016/S0032-3861(03)00011-9
26. Zhang, S.; Feng, X.; Zhu, S.; Huan, Q.; Han, K.; Ma, Y.; Yu, M., Novel toughening mechanism for polylactic acid (PLA)/starch blends with layer-like microstructure via pressure-induced flow (PIF) processing. *Materials Letters* **2013,** *98*, 238-241. https://doi.org/10.1016/j.matlet.2012.12.019
27. Yang, Z.-T.; Yang, J.-X.; Fan, J.-H.; Feng, Y.-H.; Huang, Z.-X., Preparation of super-toughened Poly(L-lactide) composites under elongational flow: A strategy for balancing stiffness and ductility. *Composites Science and Technology* **2021,** *208*, 108758. https://doi.org/10.1016/j.compscitech.2021.108758
28. Yeo, J. C. C.; Muiruri, J. K.; Tan, B. H.; Thitsartarn, W.; Kong, J.; Zhang, X.; Li, Z.; He, C., Biodegradable PHB-Rubber Copolymer Toughened PLA Green Composites with

Ultrahigh Extensibility. *ACS Sustainable Chemistry & Engineering* **2018,** *6* (11), 15517-15527. https://doi.org/10.1021/acssuschemeng.8b03978
29. Zeng, Y.; Yang, Q.-C.; Xu, Y.-T.; Ma, G.-Q.; Huang, H.-D.; Lei, J.; Zhong, G.-J.; Li, Z.-M., Durably Ductile, Transparent Polystyrene Based on Extensional Stress-Induced Rejuvenation Stabilized by Styrene–Butadiene Block Copolymer Nanofibrils. *Acs Macro Lett* **2021,** *10* (1), 71-77. https://doi.org/10.1021/acsmacrolett.0c00733
30. Zhang, S.; Zhu, S.; Han, K.; Feng, X.; Ma, Y.; Yu, M.; Reiter, G., Toughening plastics by crack growth inhibition through unidirectionally deformed soft inclusions. *Polymer* **2013,** *54* (21), 6019-6025. https://doi.org/10.1016/j.polymer.2013.08.025
31. Jasse, B.; Koenig, J. L., Orientational Measurements in Polymers Using Vibrational Spectroscopy. *Journal of Macromolecular Science, Part C* **1979,** *17* (1), 61-135. https://doi.org/10.1080/00222357908080905
32. Papkov, D.; Delpouve, N.; Delbreilh, L.; Araujo, S.; Stockdale, T.; Mamedov, S.; Maleckis, K.; Zou, Y.; Andalib, M. N.; Dargent, E.; Dravid, V. P.; Holt, M. V.; Pellerin, C.; Dzenis, Y. A., Quantifying Polymer Chain Orientation in Strong and Tough Nanofibers with Low Crystallinity: Toward Next Generation Nanostructured Superfibers. *ACS Nano* **2019,** *13* (5), 4893-4927. https://doi.org/10.1021/acsnano.8b08725
33. Zeng, Y.; Xu, Y.-T.; Zhang, J.; Xu, L.; Ji, X.; Lin, H.; Zhong, G.-J.; Li, Z.-M., Coupling Effect of Mechanical and Thermal Rejuvenation for Polystyrene: Toward High Performance of Stiffness, Ductility, and Transparency. *Macromolecules* **2021,** *54* (18), 8875-8885. https://doi.org/10.1021/acs.macromol.1c01310
34. De Focatiis, D. S. A.; Buckley, C. P., Prediction of Frozen-In Birefringence in Oriented Glassy Polymers Using a Molecularly Aware Constitutive Model Allowing for Finite Molecular Extensibility. *Macromolecules* **2011,** *44* (8), 3085-3095. https://doi.org/10.1021/ma102906z
35. De Focatiis, D. S. A.; Buckley, C. P., Craze initiation in glassy polymers: Quantifying the influence of molecular orientation. *Polymer* **2011,** *52* (18), 4045-4053. https://doi.org/10.1016/j.polymer.2011.06.044
36. Hill, M. J.; Barham, P. J.; Keller, A., On the hairdressing of shish-kebabs. *Colloid Polym Sci* **1980,** *258* (9), 1023-1037. https://doi.org/10.1007/BF01382398
37. Shih, W. K., Shrinkage modeling of polyester shrink film. *Polymer Engineering & Science* **1994,** *34* (14), 1121-1128. https://doi.org/10.1002/pen.760341405
38. Wang, Y.; Wang, S.-Q., Salient Features in Uniaxial Extension of Polymer Melts and Solutions: Progressive Loss of Entanglements, Yielding, Non-Gaussian Stretching, and Rupture. *Macromolecules* **2011,** *44* (13), 5427-5435. https://doi.org/10.1021/ma200432q
39. Wang, Y.; Wang, S.-Q., Exploring stress overshoot phenomenon upon startup deformation of entangled linear polymeric liquids. *J Rheol* **2009,** *53* (6), 1389-1401. https://doi.org/10.1122/1.3208063
40. Kramer, E. J. In *Microscopic and molecular fundamentals of crazing*, Berlin, Heidelberg, Springer Berlin Heidelberg: Berlin, Heidelberg, 1983; pp 1-56.
41. Maestrini, C.; Kramer, E. J., Craze structure and stability in oriented polystyrene. *Polymer* **1991,** *32* (4), 609-618. https://doi.org/10.1016/0032-3861(91)90472-U
42. Hou, X.; Chen, S.; Koh, J. J.; Kong, J.; Zhang, Y.-W.; Yeo, J. C. C.; Chen, H.; He, C., Entropy-Driven Ultratough Blends from Brittle Polymers. *Acs Macro Lett* **2021,** *10* (4), 406-411. https://doi.org/10.1021/acsmacrolett.0c00844

43. Likhtman, A. E.; McLeish, T. C. B., Quantitative Theory for Linear Dynamics of Linear Entangled Polymers. *Macromolecules* **2002,** *35* (16), 6332-6343. https://doi.org/10.1021/ma0200219
44. Deblieck, R. A. C.; van Beek, D. J. M.; Remerie, K.; Ward, I. M., Failure mechanisms in polyolefines: The role of crazing, shear yielding and the entanglement network. *Polymer* **2011,** *52* (14), 2979-2990. https://doi.org/10.1016/j.polymer.2011.03.055
45. Ruokolainen, J.; Fredrickson, G. H.; Kramer, E. J.; Ryu, C. Y.; Hahn, S. F.; Magonov, S. N., Effect of Thermal History and Microdomain Orientation on Deformation and Fracture Properties of Poly(cyclohexylethylene)−Polyethylene Triblock Copolymers Containing Cylindrical PE Domains. *Macromolecules* **2002,** *35* (25), 9391-9402. https://doi.org/10.1021/ma020791k
46. Tant, M. R.; Moskala, E. J.; Jank, M. K.; Pecorini, T. J.; Hill, A. J., Craze Initiation and Failure in Glassy Poly(ethylene Terephthalate): The Effects of Physical Aging with and Without Exposure to Chemical Environments. In *Structure and Properties of Glassy Polymers*, American Chemical Society: 1999; Vol. 710, pp 242-257.
47. Hill, A. J.; Heater, K. J.; Agrawal, C. M., The effects of physical aging in polycarbonate. *Journal of Polymer Science Part B: Polymer Physics* **1990,** *28* (3), 387-405. https://doi.org/10.1002/polb.1990.090280310

Table of Contents Graphic